Int. J. Electrochem. Sci., 15 **(2020)** 6257 – 6268, doi: 10.20964/2020.07.18

International Journal of
ELECTROCHEMICAL
SCIENCE
www.electrochemsci.org

SnO_2 Quantum Dots Decorated Reduced Graphene Oxide Nanosheets Composites for Electrochemical Supercapacitor Applications

Zepeng Wei[1], *Manna Liu*[2,3,4], *Hongguo Li* [1,*], *Shishuai Sun*[1,*], *Liying Yang*[2,3,4]

[1] College of Science, Tianjin University of Technology, Tianjin 300384, China
[2] School of Materials Science and Engineering, Tianjin University of Technology, Tianjin 300384, China
[3] Key Laboratory of Display Materials and Photoelectric Devices, Ministry of Education, Tianjin 300384, China
[4] Tianjin Key Laboratory of Photoelectric Materials and Devices, Tianjin 300384, China
[*]E-mail: lihongguo@tjut.edu.cn , sssdashuai@163.com

Received: 3 March 2020 / *Accepted:* 10 April 2020 / *Published:* 10 June 2020

SnO_2 quantum dots (QDs) intercalated with reduced graphene oxide nanosheet (rGO) composites are constructed by a simple hydrothermal process. The synergistic effect between the various assembly elements of the nanocomposite can compensate for the shortcomings of the individual components. The nanocomposite is attached to nickel foam to produce electrodes without adding carbon black and a binder, and the electrochemical properties of the composite electrodes are measured in 1 M Na_2SO_4 electrolyte. The results show that the prepared composite electrodes have a capacity of 253.3 F/g at a current density of 100 mA/g, and the capacity remains at 198.9 F/g even at 2000 mA/g, indicating an excellent rate capability. Moreover, cyclic voltammetry results indicate that the composite electrodes present a specific capacitance retention of 95.9% after 6000 cycles, which supports potential application in supercapacitors.

Keywords: SnO_2 quantum dots; graphene; composite materials; supercapacitor; specific capacitance

1. INTRODUCTION

Recently, supercapacitors, clean energy storage device, have received a substantial amount of attention from researchers due to their specific performance [1-3]. The type of electrode material is the main factor that determines the performance of supercapacitors. Many kinds of electrode materials are commonly used for supercapacitors, including carbon materials, various metal oxides and other conducting polymers [4-6]. Among them, electrodes made from carbon materials possess a large specific surface area, stable chemical performance, excellent electronic conductivity and wide pore size

distribution; however, they have the disadvantage of a low specific capacity [7-9]. The structures and other constraints of conductive polymers limit their application as electrode materials. In recent years, metal oxides as electrode materials have attracted a substantial amount of attention for supercapacitor applications because they have higher specific capacitances than carbon materials based on their Faraday pseudocapacitance [10-13]. However, the conductivity of transition metal oxides is poor, inevitably limiting their performance. Hence, the concept of compounding carbon materials and metal oxides has emerged as a way to enhance the performance of electrodes.

Graphene is widely used as an electrode composite material as a result of its specific electrical conductivity and thermal conductivity [14, 15]. The performance of composite electrode materials can be improved by different combinations of graphene and transition metal oxides [16, 17]. In addition, SnO_2 as an electrode material has many advantages, such as abundant reserves, environmental friendliness, and outstanding performance, and it is therefore attracting attention. However, the size of SnO_2 in SnO_2/graphene composites has ranged from 5 nm to hundreds of nanometers to date, and the dispersion of SnO_2 on graphene is not uniform [18, 19]. In fact, the size and dispersion of metal oxides that are decorated on the surface of graphene have a great influence on the properties and applications of the composites. For example, as the particle size decreases, the specific surface area increases correspondingly. When a SnO_2/graphene composite is used as a supercapacitor electrode material, it can provide additional reactive sites and improve performance. Hence, it is necessary to explore a simple and universal method to prepare ultrasmall SnO_2/graphene composites with excellent electrochemical properties.

In this paper, SnO_2 quantum dot/reduced graphene oxide nanosheet (SnO_2 QDs/rGO) composites were synthesized by an easy and economical hydrothermal method. The morphology, size and element content of the SnO_2 QDs/rGO composites were studied by transmission electron microscopy (TEM), Fourier transform infrared (FT-IR), Raman spectroscopy, X-ray photoelectron spectroscopy (XPS) and thermogravimetry (TG). The diameter of the SnO_2 quantum dots that were distributed uniformly on the rGO surface in the composites was approximately 3 nm. This material can be used as a supercapacitor electrode by directly adhering it to nickel foam without adding carbon black and a binder. The electrochemical properties of the composite were measured in 1 M Na_2SO_4 electrolyte, and the results show that the prepared composites had a capacity of 253.3 F/g when the current density was 100 mA/g (198.9 F/g even at 2000 mA/g), indicating an excellent rate capability. Moreover, cyclic voltammetry tests indicated that the composites had an available capacity retention of 95.9% after 6000 cycles.

2. EXPERIMENTAL METHODS

2.1. Materials

The graphene oxide (GO) was purchased from Nanjing Xianfeng Nanophase Materials Science and Technology Ltd. Five hydrated tin tetrachloride ($SnCl_4 \cdot 5H_2O$), hexamethylene-tetramine ($C_6H_{16}N_4$), fuming hydrochloride (HCl, 37%) and absolute ethanol analytical-grade reagents were purchased from Aladdin Industrial Corporation. Superpure water (Millipore, 18.2 MΩcm) was used throughout.

2.2. Fabrication of the SnO_2 QDs/rGO composites

The SnO_2 QDs/rGO composites were fabricated simply by a direct hydrothermal method. First, 1 mg/mL GO (15 mL) aqueous dispersion was dissolved into 9 ml of $SnCl_4 \cdot 5H_2O$ (45 mg) aqueous solution and vigorously stirred for 10 min. Afterwards, 60 mg of hexamethylene-tetramine (HMT) and 2.4 mL of fuming HCl were injected into the above suspension solution in sequence. Next, the suspension solution was placed into a 30 mL sealed stainless steel autoclave for hydrothermal reaction at 120 ℃ for 24 h. At the end of the hydrothermal reaction, the temperature of the autoclave naturally decreased to room temperature. The obtained black-colored products were retrieved by centrifugation and then washed several times with absolute ethanol and deionized water, and the final product was placed in a vacuum at 60 ℃ for 12 h. This sample is referred to as SnO_2 QDs/rGO (3:1). For comparison, different $SnCl_4 \cdot 5H_2O$ weights of 60 mg and 30 mg were used to synthesize nanocomposites with a similar method and are referred to as SnO_2 QDs/rGO (4:1) and SnO_2 QDs/rGO (2:1), respectively. Pure rGO was prepared by the same procedure without the $SnCl_4 \cdot 5H_2O$ additive.

2.3. Materials characterization

TEM analysis and high-resolution TEM (HRTEM) analysis were performed on an electron microscope (JEM-2100FEF) with an accelerating voltage of 200 kV. The FT-IR spectra were obtained with a Frontier Mid-IR FT-IR spectrophotometer by the standard KBr pellet method. The excitation wavelength of 532 nm on a HORIBA EVOLUTION Raman spectrometer was used to obtain the Raman spectra of the samples. To characterize the composites in detail, an ESCALAB 250Xi multitechnique XPS was used to confirm the element and binding energy. TG and differential thermogravimetric analysis (DTG) were conducted on an American DSC-Q600 instrument under an air atmosphere ranging from 25 ℃ to 1000 ℃ at a heating rate of 10 ℃/min.

2.4. Electrochemical measurements

First, the synthesized SnO_2 QDs/rGO materials were dissolved in anhydrous ethanol. The nickel foam was impregnated into the mixed ethanol solution so that the active material in the SnO_2 QDs/rGO could be directly dispersed on foam nickel with dimensions of 1 cm × 1 cm, thereby avoiding the use of conductive carbon black and a binder. The nickel foam adsorbed a large number of active materials as the working electrode and was placed in a vacuum oven at 60 ℃ for 12 h. Then, it was pressed to an approximately 0.1 mm thick sheet with an amount of active material of approximately 3 mg. The electrochemical properties of the as-obtained products were investigated in an electrochemical analyzer (PGSTAT 302N) using a three-electrode test system. A platinum foil (1 cm×1 cm) and silver/silver chloride (Ag/AgCl) were used as the counter electrode and reference electrode, respectively. A 1 M Na_2SO_4 aqueous solution was chosen as the electrolyte. The cyclic voltammograms (CV) were run at scan rates of 5, 10, 20, 50 and 100 mV/s, resulting in a voltage window from -0.8 to 0.4 The corresponding galvanostatic charge/discharge (GCD) tests were run at current densities of 100, 200, 500, 1000 and 2000 mA/g, resulting in a voltage window from -0.8 to 0.4 Electrochemical impedance

spectroscopy (EIS) experiments were performed at an open-circuit voltage with an amplitude of 5 mV using a frequency range from 100 kHz - 0.05 Hz. Finally, the cycling life of the SnO_2 QDs/rGO electrodes was detected by CV testing using a scan rate of 50 mV/s for 6000 cycles.

3. RESULTS AND DISCUSSION

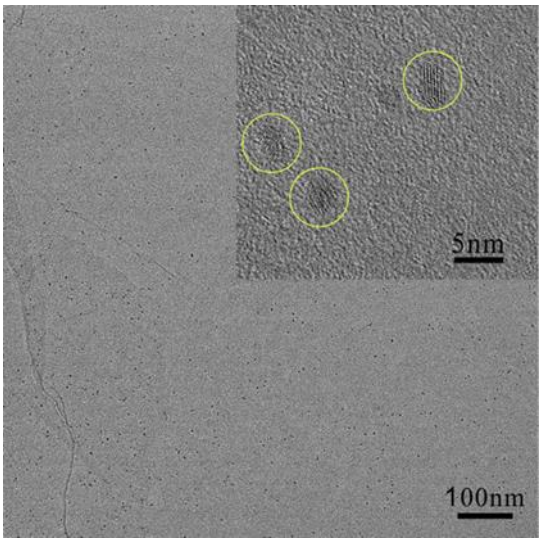

Figure 1. TEM and HRTEM (insert) of the SnO_2 QDs/rGO (3:1) composite

The morphology and microstructure of the SnO_2 QDs/rGO (3:1) composite were characterized by TEM and HRTEM. It can be seen from Fig. 1 that many uniform SnO_2 QDs decorated the rGO surface well with a diameter of ~3 nm. As is known, two-dimensional of graphene is easy to stack, resulting in blockage of the electrolyte transmission channel when it is used as an electrode. The SnO_2 QDs loaded on the surface of rGO can effectively solve this problem [20-22]. Moreover, the thin graphene layer in the composites can effectively prevent the aggregation of small SnO_2 QDs and improve the electronic transmission performance [23-25]. Thus, the porosity of the composite was improved, and the exposure of the electrode materials to the electrolyte increased. The above structural characteristics of the composites improved their electrochemical properties. Moreover, even after ultrasonic treatment, the SnO_2 QDs were closely attached to the surface of the rGO layer, which improved the cycling stability of the materials. The figure displays HRTEM images of the SnO_2 QDs/rGO (3:1) composite. The crystal lattice spacing was 0.337 nm, corresponding to the (110) face of the SnO_2 rutile phase. It was shown that tetragonal rutile SnO_2 was formed in the synthesized product.

To determine the reduction degree of the GO in the SnO_2 QDs/rGO composites, FT-IR studies were carried out. The FT-IR spectra of the GO and SnO_2 QDs/rGO composites are shown in Fig. 2A. For the GO, various functional groups were easily found, such as C-O, O-H, and C=O, which were located at 1076, 1404 and 1631 cm^{-1}, respectively [18, 26, 27]. An obvious 3436 cm^{-1} peak was attributed to the hydroxyl groups or the adsorbed bound water in the material [28]. These oxygen functional groups were the active sites that adsorbed the metal cations on the surface of GO. These functional groups on the surface of GO were reduced by a long reaction time under high-temperature conditions. Compared with the peaks for the GO, we can clearly observe that the peak from the oxygen functionalities in the

SnO_2 QDs/rGO composites were obviously weakened, illustrating that the GO was effectually reduced to rGO during the composite preparation.

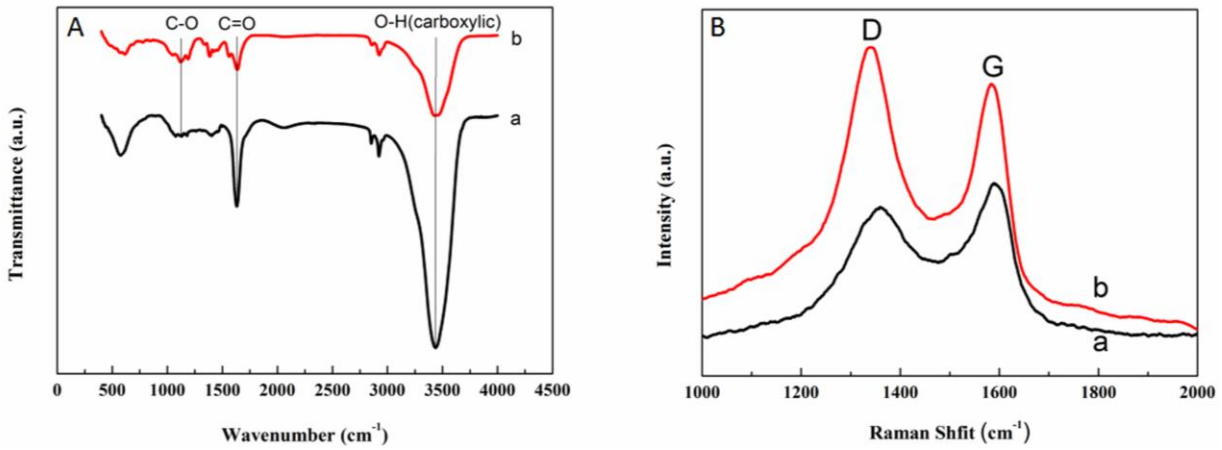

Figure 2. FTIR (A) and Raman (B) spectra of GO (a) and SnO_2 QDs/rGO (3:1) composite (b)

To demonstrate the significant structural differences between the GO and SnO_2 QDs/rGO, the Raman spectroscopy was used. In Fig. 2B, it can be seen that all of the Raman spectra contained both the D band peak at 1358 cm^{-1} and the G band peak at 1596 cm^{-1} in both materials. The disorder in carbon materials can be analyzed by comparing the intensity of the D and G bands [29-31]. In Fig. 2B, the I_D/I_G ratios were 0.89 and 1.12 for the GO and SnO_2 QDs/rGO, respectively. The I_D/I_G ratio for the SnO_2 QDs/rGO composite was larger than that for the GO, indicating that the average size of the sp^2 decreased due to the GO changing to rGO during the reaction [32]. At the same time, these results indicate that a high concentration of structural defects existed on the surface of the rGO in the SnO_2 QDs/rGO composite. The above results demonstrate that SnO_2 quantum dots were effectively combined with the rGO nanosheets. Moreover, these characteristics improved the electrochemical performance of the composites as electrode materials.

To further determine the chemical compositions of the SnO_2 QDs/rGO composites and the reduction degree of GO in the composites, XPS analyses were performed. Fig. 3A shows the XPS spectra of the SnO_2 QDs/rGO composite. We can clearly see that the sample contained C, O and Sn elements. The Sn peaks were derived from SnO_2, and C1s peaks were derived from the existence of rGO. Fig. 3B shows the Sn $3d_{3/2}$ and Sn $3d_{5/2}$ peaks for the SnO_2 QDs/rGO composites at 495.7 and 487.5 eV, respectively, which indicates the presence of Sn^{4+} [33]. There were no other peaks that indicated other chemical states of Sn, proving the presence of SnO_2 in the composite materials. The resolved curves of the C1s peaks for the GO and the SnO_2 QDs/rGO composites are shown in Fig. 3C and D, respectively. In Fig. 3C, we can see peaks related to C-C, C-O, C=O and O-C=O centered at 284.8, 286.2, 288.0 and 289.2 eV, respectively [34]. Moreover, in Fig. 3D, we can see that the same functionalities were present in the composites. However, the intensity of the C-C peak was obviously enhanced, while the intensity of the C-O and C=O peaks remarkably decreased, and the O-C=O peak almost disappeared in the SnO_2 QDs/rGO composites compared with that for the pure GO. The XPS results further illustrate that most

of the GO was reduced to rGO during the course of the reaction. This result is in accord with the FTIR results.

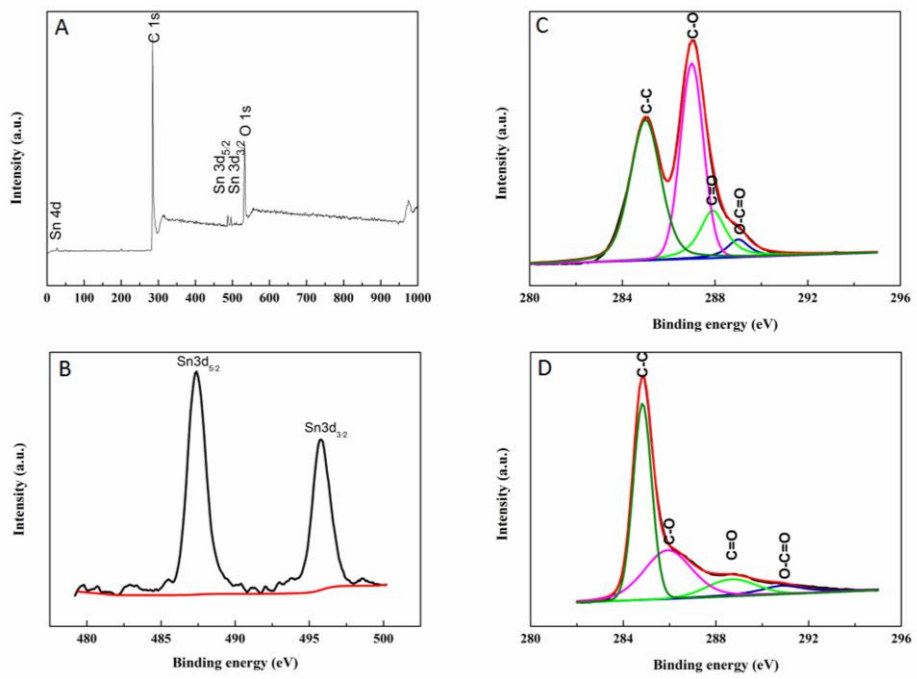

Figure 3. XPS survey spectrum of the SnO_2 QDs/rGO (3:1) composite (A), XPS spectra of Sn 3d in the SnO_2 QDs/rGO (3:1) composite (B), C1s in the pure GO (C) and C1s in the SnO_2 QDs/rGO (3:1) composite (D)

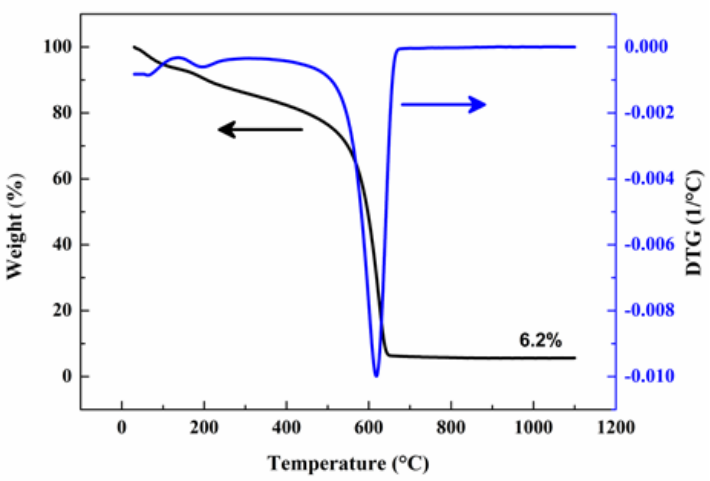

Figure 4. TG and DTG curves of the SnO_2 QDs/rGO (3:1) composites

To determine the mass loading of the SnO_2 in the SnO_2 QDs/rGO composites, TG and DTG analyses of the composites were performed. Fig. 4 shows the TG and DTG curves for the SnO_2 QDs/rGO composites. The calculated mass loading of SnO_2 was 6.2% in the SnO_2 QDs/rGO composites. In fact, the formation mechanism of the SnO_2 QDs/rGO nanocomposites should be understood to further explore

the related materials. Based on the system characterization, the probable formation mechanism can be illustrated as follows. During the reaction process, Sn^{4+} ions were first bonded covalently to the surface of GO through electrostatic interactions with the assistance of various GO surface functional groups [18,19]. With the addition of HMT, many OH^- ions appeared in suspension, and then OH^- ions aided in the formation of $Sn(OH)_4$ by combining with Sn^{4+} ions [35]. During the hydrothermal treatment, the remanent oxygen functionalities on the surfaces of GO were further reduced, and $Sn(OH)_4$ transformed into SnO_2. The addition of HCl controlled the concentration of OH^- ions in the reaction system to control the growth of SnO_2 [36]. Finally, the SnO_2 QDs/rGO composites were prepared.

The electrochemical properties of the prepared SnO_2 QDs/rGO composites for use in supercapacitors were investigated by various electrochemical measurements in 1 M Na_2SO_4 aqueous electrolyte. Fig. 5A shows the GCD curves for different mass ratios of the SnO_2 QDs/rGO composites running at voltage windows from -0.8 to 0.4 V when the current density was 500 mA/g. Obviously, the SnO_2 QDs/rGO (3:1) composite electrode had a higher specific capacitance than the other materials due to its longest charge and discharge time during the GCD testing at the same current density. Fig. 5B shows the GCD curves for the SnO_2 QDs/rGO (3:1) composite electrodes under 100, 200, 500, 1000 and 2000 mA/g. The discharge time for the composite electrode at a high current density is smaller than that at a low current density, indicating a decrease in the specific capacitance with an increase in the current. In addition, the GCD curves of the composite electrodes were asymmetric, and the voltage drop in the curves was not obvious, which also indicates typical pseudocapacitive properties and excellent electronic transmission characteristics [37-38].

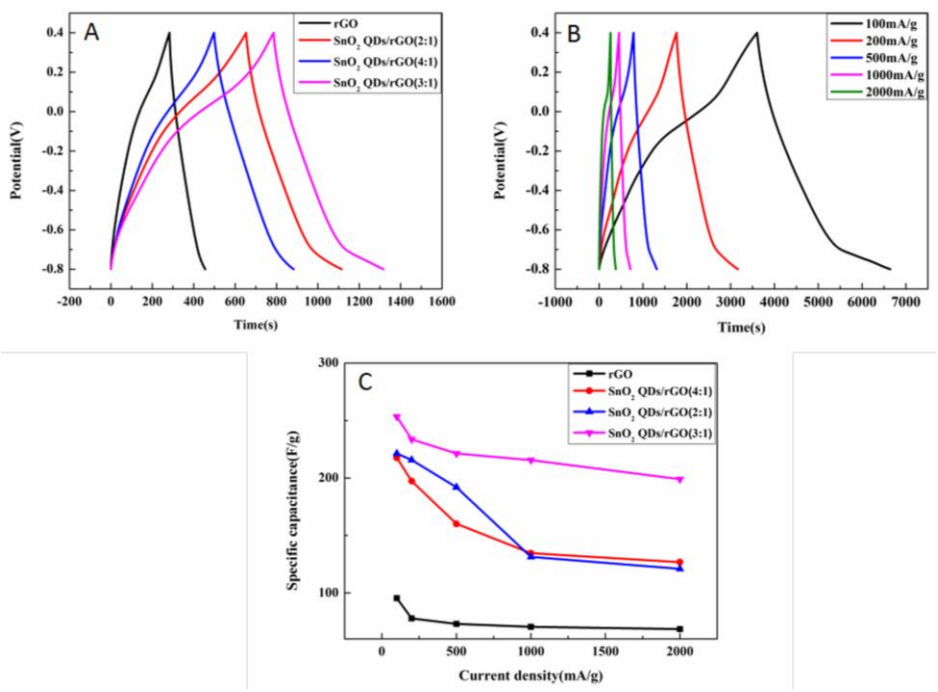

Figure 5. GCD profiles for the ultrafine rGO and SnO_2 QDs/rGO composites with different mass ratios when the current density was 500 mA/g (A); GCD profiles of the SnO_2 QDs/rGO composites at 100, 200, 500, 1000 and 2000 mA/g (B); capacitance values for the rGO and SnO_2 QDs/rGO composites at different current densities (C)

Based on the GCD curves, we can quantitatively analyze the performance of the electrode by the following equation [18]:

$$Cs = \frac{It}{\Delta Vm}, \qquad (1)$$

In this equation, *Cs*, *I*, *t*, *ΔV* and *m* are the specific capacitance (F/g), constant current (A), discharge time (s), discharge voltage range (V) and mass of the active material (g), respectively. According to this equation, the maximum Cs values for the SnO_2 QDs/rGO (3:1), SnO_2 QDs/rGO (2:1), SnO_2 QDs/rGO (4:1) and rGO electrodes were 253.3, 221.3, 217.6 and 95.4 F/g, respectively, at a current density of 100 mA/g, as shown in Fig. 5C. Obviously, the maximum specific capacitance of the SnO_2 QDs/rGO (3:1) composite electrodes was higher than that of rGO and other composites, illustrating that the capacitive performance of the SnO_2 QDs/rGO (3:1) composite electrodes was remarkably improved due to the combination of the advantages of the SnO_2 quantum dots and rGO. As shown in Fig. 5C, the calculated specific capacitance of all electrodes decreased when the current density increased from 100 to 2000 mA/g. In fact, when the electrode materials were run at high current, the ions in the electrolyte, such as H^+ and Na^+, could not effectively transfer into the inner structure of the electrode, lowering the performance of the electrode [39]. At a low current density, a high performance can be obtained from a sufficient Faraday reaction due to the large number of ions diffusing into the inner structure of the electrode [40-43].

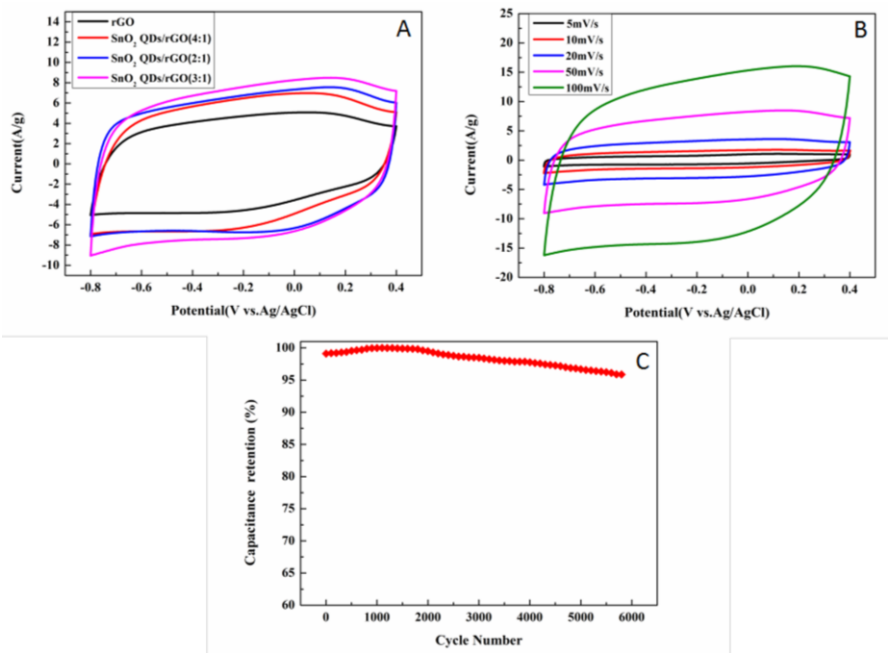

Figure 6. CV profiles of the rGO and SnO_2 QDs/rGO composites with different mass ratios when the scan rate was 50 mV/s (A); CV curves of the SnO_2 QDs/rGO (3:1) composite (B); cycling life of the SnO_2 QDs/rGO (3:1) composite using 50 mV/s for 6000 cycles during the CV test (C)

The CV curves for the synthesized SnO_2 QDs/rGO composites with different mass ratios are plotted in Fig. 6A for a scan rate of 50 mV/s and a voltage window range from -0.8 to 0.4 V. The results show that the current values and integral area of the CV curve for the SnO_2 QDs/rGO (3:1) composite

electrode were larger than those of the other materials when the scan rate was the same. It can be deduced that the SnO_2 QDs/rGO (3:1) composite demonstrated outstanding performance, which is in accordance with the GCD results. The CV curves of the SnO_2 QDs/rGO (3:1) composite electrode run at scan rates of 5, 10, 20, 50, and 100 mV/s are also shown in Fig. 6B. With increasing scan rate, the peak current value showed an upward trend, and the curves maintained the same shape, indicating that the electrochemical properties of the SnO_2/rGO (3:1) composite electrode were stable in this potential range. Moreover, the curves for the SnO_2 QDs/rGO (3:1) composite electrode had a rectangular shape, which is the common effect from the SnO_2 pseudocapacitance and rGO double-layer capacitance. The SnO_2-related reaction for the charge storage mechanism can be expressed as follows [44]:

$$(SnO_2)_{surface} + Na^+ + e^- \leftrightarrow (SnO_2^- - Na^+)_{surface} \quad (2)$$

The electrochemical cyclic stability of the SnO_2 QDs/rGO (3:1) composite electrodes was further investigated by CV using the same scan rate of 50 mV/s over 6000 cycles. From Fig. 6C, it can be seen that the SnO_2 QDs/rGO (3:1) composite still had 95.9% capacitance retention after 6000 cycles. This result indicates that the SnO_2 QDs/rGO (3:1) composite electrode had an excellent cycle life and can be applied as an electrode for high-performance supercapacitors.

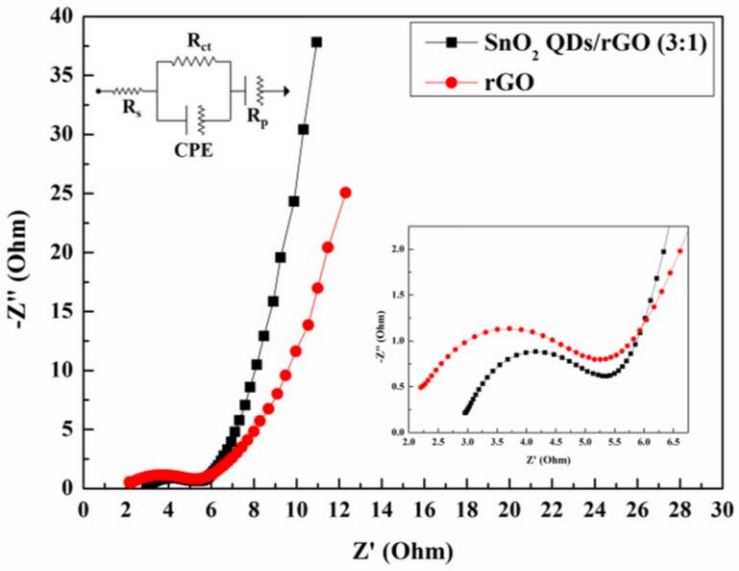

Figure 7. EIS for the rGO and SnO_2 QDs/rGO (3:1) composite

EIS experiments were carried out to analyze the inner resistance of the SnO_2 QDs/rGO composites. Fig. 7 shows the Nyquist plot of the SnO_2 QDs/rGO (3:1) composite and rGO. The illustration in the top left corner shows the corresponding equivalent circuit diagram for the EIS results, and the illustration in the bottom right corner shows an enlargement of the high-frequency region of the plot. The results show that there were semicircles and straight lines located in the high-frequency region and low-frequency region, respectively. The corresponding equivalent circuit diagram is composed of a charge-transfer resistance (R_{ct}), bulk solution resistance (R_s), capacitor element (R_p) and constant phase element (CPE). The R_{ct} and Rs values were highly dependent on the semicircle in the high-frequency region. In the high-frequency region (inset in Fig. 7), it can be seen that the R_s of the SnO_2 QDs/rGO

(3:1) composite (2.9 Ω) was larger than that of the rGO (2.1 Ω), which was obviously due to the poor conductivity of SnO_2. However, the diameter of the semicircle in the EIS curve for the SnO_2 QDs/rGO (3:1) composite was smaller than that for the rGO, indicating an excellent electric transport path. The straight line in the low-frequency range indicates the capacitance characteristics of the charge-discharge mechanism [45-47]. The straight line for the SnO_2 QDs/rGO (3:1) composite is more vertical than that for the rGO material, also indicating a good ion diffusion rate. Based on our results, we also deduced that the outstanding performance of the SnO_2 QDs/rGO composite originated from the combined effects of the ultrafine SnO_2 and rGO. The electrichemical performance of SnO_2 and graphene-related nanocomposites reported in recent years were shown in Table 1, and our synthesized material showed excellent performance compared with those of other references.

Table 1. The comparison of electrochemical performance between different SnO_2 and graphene-related materials.

Material	Electrolyte	Cycling Performance	Specific capacitance	Ref.
Graphene-SnO_2	1M H_2SO4	-	43 F/g at 1 mV/s	[17]
SnS_2-SnO_2	0.5M Na_2SO_4	92% after 2800 cycles	149 F/g at 2A/g	[12]
SnO_2/CNT	2 M KCl	75% after 500 cycles	188.42 F/g at 2 mV/s	[47]
Graphene/SnO_2/PEDOT	1M H_2SO4	100% after 5000 cycles	188 F/g at 1 mV/s	[48]
Zn doped SnO_2	6 M KOH	-	206 F/g at 5 mV/s	[45]
CNFs/SnO_2	3M KOH	-	225.4 F/g at 1A/g,	[46]
SnO_2/CC	0.5 M $LiNO_3$	-	247 F/g at 1A/g,	[49]
SnO_2 QDs/rGO (3:1)	1M Na_2SO_4	95.9% after 6000 cycles	253.3 F/g at 100 mA/g	This work

4. CONCLUSION

SnO_2 QDs/rGO composites were successfully constructed as electrode materials for supercapacitors. The TEM analysis illustrated that the SnO_2 quantum dots were uniformly deposited on the wrinkled rGO, and HRTEM analysis indicated the tetragonal structure of SnO_2 in the composites. The size of the SnO_2 that decorated the rGO surface was only 3 nm. The composites were used as electrodes in a three-electrode system after adhering to nickel foam to avoid a complicated preparation procedure that involved the use of carbon black and a binder. The electrochemical properties of the composite were measured in 1 M Na_2SO_4 electrolyte, and the results showed that the prepared composites had a capacity of 253.3 F/g when the current density was 100 mA/g (198.9 F/g even at 2000 mA/g), indicating excellent rate capability. Moreover, cyclic voltammetry measurements indicated that the composites still had a 95.9% capacity retention after 6000 cycles, implying an outstanding cycle life.

ACKNOWLEDGEMENTS
The authors are grateful to the financial support from the National Natural Science Foundation of China (No.11504267, 51402214) and Tianjin NSFC (No. 17JCYBJC21000).

References

1. R.R. Salunkhe, Y.H. Lee, K.H. Chang, J.M. Li, P. Simon, J. Tang, N.L. Torad, C.C. Hu, Y. Yamauchi, *Chem. Eur. J*, 20 (2014) 13838.
2. A. Das, S. Deshagani, R. Kumar, M. Deepa, *ACS Appl. Mater. Interfaces*, 10 (2018) 35932.
3. G.T.Xiang, Y. Meng, G.M.Qu , J.M. Yin, B.Teng, Q.Wei, X.J. Xu, *Sci. Bull*, 65 (2020) 443.
4. H. Kim, M.E. Fortunato, H. Xu, J.H. Bang, K.S. Suslick, *J. Phys. Chem*. C, 115 (2011) 20481.
5. J. Ge, G. Cheng, L. Chen, *Nanoscale*, 3 (2011) 3084.
6. R. Liang, H. Cao, D. Qian, *Chem. Commun*, 47 (2011) 10305.
7. H.R. Byon, S.W. Lee, S. Chen, P.T. Hammond, Y.S. Horn, *Carbon*, 49 (2011) 457.
8. X. He, Y. Geng, J. Qiu, M. Zheng, X. Zhang, H. Shui, *Energy Fuels*, 24 (2010) 3603.
9. Z. Gao, J. Wang, Z. Li, W. Yang, B. Wang, M. Hou, Y. He, Q. Liu, T. Mann, P. Yang, M. Zhang, L. Liu, *Chem. Mater*, 23 (2011) 3509.
10. J. Zhu, J. Jiang, J. Liu, R. Ding, H. Ding, Y. Feng, G. Wei, X. Huang, *J. Solution Chem*, 184 (2011) 578.
11. M. Zhang, D. Lei, Z. Du, X. Yin, L. Chen, Q. Li, Y. Wang, T. Wang, *J. Mater. Chem*, 21 (2011) 1673.
12. P.Asen , M. Haghighi, S. Shahrokhian, N. Taghavinia, *J. Alloys Compd*, 782 (2019) 38.
13. J. Xiao, S. Yang, *RSC Adv*, 1 (2011) 588.
14. K. Liu, Y. Yao, T. Lv, H.L. Li, N. Li, Z.L.Chen, G.J. Qian, T. Chen, *J. Power Sources*, 446 (2020) 227355.
15. M.J. Allen, V.C. Tung, R.B. Kaner, *Chem. Rev*, 110 (2009) 132.
16. G. He, J. Li, H. Chen, J. Shi, X. Sun, S. Chen, X. Wang, *Mater. Lett* , 82 (2012) 61.
17. *F.H. Li, J.F. Song, H.F. Yang, S.Y. Gan, Q.X. Zhang, D.X. Han, A.Ivaska, L. Niu, Nanotechnology*, 20 (2009) 455602
18. B. Wang, D. Guan, Z. Gao, J. Wang, Z. Li, W. Yang, L. Liu, *Mater. Chem. Phys*, 141 (2013) 1.
19. C. Xu, J. Sun, L. Gao, *J. Mater. Chem*, 22 (2012) 975.
20. L.S. Zhang, L.Y. Jiang, H.J. Yan, W.D. Wang, W. Wang, W.G. Song, Y.G. Guo, L.J. Wan, *J. Mater. Chem*, 20 (2010) 5462.
21. P. Lian, X. Zhu, H. Xiang, Z. Li, W. Yang, H. Wang, *Electrochim. Acta*, 56 (2010) 834.
22. Z. Du, X. Yin, M. Zhang, Q. Hao, Y. Wang, T. Wang, *Mater. Lett*, 64 (2010) 2076.
23. X. Wang, X. Zhou, K. Yao, J. Zhang, Z. Liu, *Carbon*, 49 (2011) 133.
24. H. Liu, D. Long, X. Liu, W. Qiao, L. Zhan, L. Ling, *Electrochim. Acta*, 54 (2009) 5782.
25. C. Chen, L. Wang, Y. Liu, Z. Chen, D. Pan, Z. Li, Z. Jiao, P. Hu, C.H. Shek, C.M.L. Wu, J.K.L. Lai, M. Wu, *Langmuir*, 29 (2013) 4111.
26. M. Saranya, R. Ramachandran, P. Kollu, S.K. Jeong, A.N. Grace, *RSC Adv*, 5 (2015) 15831.
27. C. Xu, X. Wang, J. Zhu, *J. Phys. Chem*. C, 112 (2008) 19841.
28. L. Qiu, X. Yang, X. Gou, W. Yang, Z.F. Ma, G.G. Wallace, D. Li, *Chem. Eur. J*, 16 (2010) 10653.
29. Y. Song, Z. Li, K. Guo, *Nanoscale*, 8 (2016) 15671.
30. M. Zhou, J. Tang, Q. Cheng, G. J. Xu, P. Cui, L.C. Qin, *Chem. Phys. Lett*, 572 (2013) 61.
31. C. T. J. Low, F. C. Walsh, M. H. Chakrabarti, M. A. Hashim, M. A. Hussain, *Carbon*, 54 (2013) 1.
32. R.F. Hu, J. Zhao, J.P. Zheng, *Mater. Lett*, 197 (2017) 59.
33. S. S. Mali, C. S. Shim, H. Kim, C. K. Hong, *J. Mater. Chem*. A, 4 (2016) 12158.
34. S. Stankovich, R. D. Piner, X. Chen, N. Q. Wu, S. B. T. Nguyen, R. S. Ruoff, *J. Mater. Chem*, 16

(2006) 155.
35. Y. K. Wang, Y. S. Liu, J. M. Zhang, *J. Nanopart. Res*, 17 (2015) 420.
36. G. C. Xi, J. H. Ye, *Inorg. Chem*, 49 (2010) 2302.
37. H. F. Su, T. Wang, S. Y. Zhang, J. M. Song, C. J. Mao, H. L. Niu, B. K. Jin, J. Y. Wu, Y. P. Tian, *Solid State Sci*, 14 (2012) 677.
38. B. S. Yin, Z. B. Wang, S. W. Zhang, C. Liu, Q. Q. Ren, K. Ke, *ACS Appl. Mat. Interfaces*, 8 (2016) 26019.
39. D. S. Yu, L. M. Dai, *J. Phys. Chem. Lett*, 1 (2010) 467.
40. J. Zhu, J. H. He, *ACS Appl. Mat. Interfaces*, 4 (2012) 1770.
41. S. Z. Ren, Y. Yang, M. L. Xu, H. M. Cai, C. Hao, X. Z. Wang, *Colloids Surf.* A, 444(2014) 26.
42. Z. J. Li, T. X. Chang, G. Q. Yun, Y. Jia, *Powder Technol*,224(2012) 306.
43. Z. Y. Luo, Y. H. Zhu, E. H. Liu, T. T. Hu, Z. P. Li, T. T. Liu, L. C. Song, *Mater. Res. Bull*,60 (2014) 105.
44. Y. D. Zhang, Z. Hu, Y. R. Liang, Y. Y. Yang, N. An, Z. M. Li, H. Y. Wu, *J. Mater. Chem. A*, 3 (2015) 15057.
45. S. Suthakaran, S. Dhanapandian, N. Krishnakumar, N. Ponpandian, *J. Phys. Chem. Solids*, 141 (2020) 109407.
46. Y.X. Luan, G.D. Nie, X.W. Zhao , N. Qiao , X.C. Liu , H. Wang, X.N. Zhang, Y.Q. Chen, Y.Z. Long,
47. C.H. Xu, J.Z. Chen, *Ceram. Int*, 42(2016)14287.
48. W.J. Wang, W. Lei, T.Y. Yao, X.F. Xia, W.J. Huang, Q.L. Hao, X. Wang, *Electrochim. Acta*, 108 (2013)118.
49. Y.D. Zhang, Z.G. Hu, Y.R. Liang, Y.Y. Yang, N. An, Z.M. Li, H.Y. Wu, *J. Mater. Chem. A*,3(2015)15057-15067